Antimony isotope fractionation during Sb(V) and Sb(III) adsorption on secondary Fe-minerals (schwertmannite, ferrihydrite) typical of mine waters

Colin Ferrari, Eléonore Resongles, Rémi Freydier, Corinne Casiot

Antimony isotope fractionation during Sb(V) and Sb(III) adsorption on secondary Fe-minerals (schwertmannite, ferrihydrite) typical of mine waters

Colin Ferrari[a], *Eléonore Resongles*[*a], *Rémi Freydier*[a], *and Corinne Casiot*[a]

[a]HydroSciences Montpellier, Univ. Montpellier, CNRS, IRD, Montpellier, France

***Corresponding author:**

Mailing address: Université Montpellier – HydroSciences
Bâtiment HYDROPOLIS
15 avenue Charles Flahault
34090 Montpellier
Email: eleonore.resongles@ird.fr

ABSTRACT

The application of antimony (Sb) isotopes as tracers for Sb environmental cycling is currently limited. Indeed, there is a lack of knowledge of isotope fractionation factors associated with key (bio-) geochemical processes controlling its behaviour in surface environments. This study investigated the equilibrium isotope fractionation generated by Sb(V) and Sb(III) sorption on two iron minerals typical of acid mine drainage (AMD) impacted streams, ferrihydrite and schwertmannite, under controlled conditions of pH and solid to liquid ratio. Sorption behaviour and Sb isotope fractionation were similar for the different mineral phases and Sb oxidation degrees, with fractionation factors $\Delta^{123}Sb_{solid\text{-}solution}$ of -0.25 ± 0.08 ‰ for Sb(III) and -0.34 ± 0.08 ‰ for Sb(V) adsorbed on ferrihydrite and -0.36± 0.06 ‰ for Sb(III) and -0.27 ± 0.03 ‰ for Sb(V) adsorbed on schwertmannite. The pH and initial Fe:Sb ratio did not significantly affect the $\Delta^{123}Sb_{solid\text{-}solution}$ value under the experimental conditions. The light ^{121}Sb isotope was preferentially adsorbed on the mineral phases, following an equilibrium closed system between dissolved and adsorbed Sb species. This fractionation may be related to the apparition of iron as the second closest neighbour which distorts the $Sb(OH)_3$ or $Sb(OH)_6^-$ atomic polyhedron. This study confirms that Sb equilibrium isotope fractionation occurs during sorption of Sb(III) and Sb(V) onto secondary iron minerals and suggests that the pH and redox of Sb do not exert significant effect. pH and redox conditions are important parameters which control Sb mobility in AMD streams, therefore, the study provides data for interpreting Sb isotope signatures in mine waters.

Keywords : Antimony isotopes – Equilibrium isotope fractionation – Iron oxyhydroxides – Adsorption – Mining Environments

1. INTRODUCTION

Antimony (Sb) is a critical element for the modern industry, mainly for its application as a flame retardant in plastics and its use in lead alloys (European Commission, 2020; U.S. Geological Survey, 2022). As a consequence, Sb mine production has peaked over the last twenty years with an annual world production of 142 to 193 kT (2004-2018 data, U.S. Geological Survey, 2018) leading to a general increase of Sb levels in the environment (He *et al.*, 2019; Bolan *et al.*, 2022). In surface waters, dissolved Sb concentrations are usually low (< 1 $\mu g.L^{-1}$) and the highest concentrations of this toxic element (up to ~29 $mg.L^{-1}$) are found in streams in sulphide mining areas (Wang *et al.*, 2011; Guo *et al.*, 2018; Hao *et al.*, 2021).

In mining Sb-rich environments, the alteration of sulphides produces acid leachates (acid mine drainage, AMD), that contain high concentrations of iron and sulphate. These constituents precipitate subsequently to iron oxidation and AMD neutralization by river water; they form secondary minerals, hydrous ferric oxides (HFO) and ferric hydroxysulphates (Bigham *et al.*, 1996). Due to their high specific surface area and positive surface charges, these minerals are good sorbents for antimony (Leuz *et al.,* 2006; Mitsunobu *et al.,* 2006; Mitsunobu *et al.*, 2010; Guo *et al.*, 2014; Qi and Pichler, 2016, 2017; Schoepfer *et al.*, 2021) and therefore, they control the transport of Sb in the rivers receiving mining effluents (Filella, Williams and Belzile, 2009; Manaka *et al.*, 2007; Nagano *et al.*, 2011; Resongles *et al.*, 2013; Johnston *et al.*, 2020, Rastegari et al., 2022, Shan et al., 2023). Among the solid phases most commonly encountered in AMD streams and downstream rivers, are schwertmannite ($Fe_8O_8(OH)_{8-2x}SO_{4x}\bullet\ nH_2O$, $1 < x < 1.75$) in the pH range 2-4.5 and ferrihydrite ($Fe_5HO_8{,}4H_2O$) at pH ≥ 6.5 (Bigham et al., 1996; Schoepfer *et al.*, 2021). The oxidative dissolution of stibnite (Sb_2S_3), the main Sb ore, can lead to the release of Sb in water in its trivalent form, Sb(III) (Biver and Shotyk, 2012). Besides oxidation, attenuation of dissolved Sb(III) concentrations in mine waters is attributable to Sb(III) adsorption on Fe secondary minerals (Beauchemin *et al.*, 2012; Resongles *et al.*, 2013). These field observations were further supported by experimental adsorption studies which showed that Sb(III) is more efficiently adsorbed on ferrihydrite and schwertmannite than Sb(V) (Qi and Pichler, 2016; Li *et al.*, 2016).

Antimony isotope system (^{121}Sb and ^{123}Sb) is emerging due to its strong potential as a geochemical tracer (Teng *et al.,* 2017; Johnson *et al.*, 2022). Several studies were focused on sample preparation and optimization of Sb isotope ratio analysis by Multi Collector Inductively Coupled Plasma Mass Spectrometry MC-ICP-MS (Asaoka *et al.*, 2011; Lobo *et*

al., 2012; Liu *et al.*, 2020; Kaufmann *et al.*, 2021; Ferrari *et al.*, 2021; Li *et al.*, 2021; Sun *et al.*, 2021). Others provided data on Sb isotope signatures in primary Sb minerals, manufactured materials and environmental samples (Rouxel *et al.*, 2003; Lobo *et al.*, 2013, 2014; Degryse *et al.*, 2015, 2020; Resongles *et al.*, 2015; Ferrari *et al.*, 2021). However, to date Sb isotope fractionation factors associated with geochemical processes such as adsorption are poorly known, limiting the development of Sb isotopes as environmental tracers.

The extent of isotope fractionation occurring during metal sorption generally remains limited (< 1 ‰) (Wiederhold, 2015; Komárek *et al.*, 2021). Both light and heavy isotope enrichments in adsorbed species have been observed in metal sorption studies on oxyhydroxides, depending on the bonding environment of adsorbed and aqueous metal species (Komárek *et al.*, 2021). Isotope fractionation generated by sorption also varies with the mineralogy (Komárek *et al.*, 2021), for example in the case of the sorption of Zn adsorbed on ferrihydrite and goethite (Juillot *et al.*, 2008), of Mo on Fe-(oxyhydr)oxides, for which the fractionation increases in the order magnetite < ferrihydrite < goethite < hematite (Goldberg *et al.*, 2009), or Sb(V) adsorbed on alumina < ferrihydrite < hematite and goethite (Zhou et al., 2022, 2023). This mineral effect can be related both to mineral surface speciation and solution chemistry (Goldberg *et al.*, 2009). A number of studies showed that the outer-sphere complexation generates lower fractionation than the inner-sphere complexation due to the control of complexing ligands by weak electrostatic forces on the surface and their participation in anion exchange (Essington and Stewart, 2018). The inner-sphere complexation is subject to stronger bonding (Essington and Stewart, 2018; Zhou *et al.*, 2022, 2023). Therefore, the bonding environment of Sb in the solid and aqueous phases is of prime interest to interpret the observed Sb isotope fractionation factors. Antimony adsorption mechanisms have been investigated at the molecular level on various iron minerals including ferrihydrite, schwertmannite, hematite and goethite (Scheinost *et al.*, 2006; Mitsunobu *et al.*, 2010; Guo *et al.*, 2014; Essington and Stewart, 2018; Zhou *et al.*, 2023; Shan et al., 2023). Antimony(V) forms inner-sphere complexes at the surface of ferrihydrite by edge-sharing and edge and corner-sharing independently from pH or surface coverage (Mitsunobu *et al.*, 2010; Guo *et al.*, 2014; Zhou *et al.*, 2023). For schwertmannite, Sb adsorption studies have mainly focused on its use as a sorbent for the treatment of water contaminated with Sb (Schoepfer *et al.*, 2021). An experimental and modeling study suggested the formation of inner-sphere complexes between Sb(V) and schwertmannite (Nagano et *al.*, 2011). This was recently confirmed by a study at the molecular scale revealing edge-sharing and corner-sharing complexation between Sb(V) and schwertmannite accompanied by its incorporation in the

mineral structure depending on pH and Sb loading (Shan et al., 2023). Recently, two experimental studies (Zhou *et al.*, 2022, 2023) focused for the first time on Sb isotope fractionation during sorption on aluminium and iron oxy(hydro)xides. The authors found that Sb(V) adsorption on aluminium oxides does not produce significant equilibrium Sb isotope fractionation (Zhou et al., 2022). On the other hand, a significant equilibrium isotope fractionation was observed as a result of Sb(V) adsorption on ferrihydrite, hematite and goethite (-1.14 ‰ < $\Delta^{123}Sb_{\text{solid-solution}}$ < -0.49 ‰). The difference in the magnitude of the fractionation factors among the three Fe minerals was ascribed to different inner-sphere adsorption mechanisms of Sb(V) on ferrihydrite (formation of edge and corner-sharing complexes) and hematite or goethite (formation of edge-sharing complexes) (Zhou *et al.*, 2023). Therefore, these pioneering studies evidenced that the extent of Sb isotope fractionation generated by adsorption depends on the mineral phases and Sb adsorption modes as previously reported for other elements such as Cd, Cu, Ni, Se or Zn (Xu *et al.*, 2020; Komárek *et al.*, 2021).

Antimony isotope fractionation generated by adsorption processes needs further investigation to quantify fractionation factors involving other environmentally relevant mineral phases and Sb(III) species. In particular, in the perspective of using Sb isotopes to track pollution sources in watersheds impacted by sulphide ore mining, and/or to unravel the processes Sb undergoes in mine-impacted streams, it is essential to document Sb isotope fractionation during sorption of Sb(III) and Sb(V) on secondary iron minerals typical of AMD streams.

In this context, the objective of this study was to complement recent studies by focusing on the quantification of the isotope fractionation factors at equilibrium between dissolved and adsorbed Sb species, both in a trivalent and pentavalent Sb form, on two mineral phases widely distributed in sulphide mining environments, ferrihydrite and schwertmannite, and to make hypothesis regarding the possible origin of the observed fractionation based on existing knowledge on adsorption mechanisms.

2. MATERIAL AND METHODS

2.1. Reagents and materials

Ultrapure water (Milli-Q®, resistivity > 18.2 MΩ.cm, Q-POP Element system, Millipore) was used for all experiments and reagent preparation. All consumables (e.g., sample bottles, tubes, SPE cartridge, pipette tips…) were soaked in 10 % w/w analytical grade HCl for 48 h and rinsed three times with ultrapure water before use. $Fe(NO_3)_3,9H_2O$ (Sigma-Aldrich®), $FeSO_4.7H_2O$ (Sigma-Aldrich®), 30 % w/w H_2O_2 (analytical grade, Fisher Scientific®), 1 $mol.L^{-1}$ KOH (Merck®) were used for the synthesis of schwertmannite and 2-line ferrihydrite. $NaNO_3$ (Merck®) and NaOH (99.99 % trace metal basis, Sigma-Aldrich®) were used for adsorption experiments. 30 % w/w HCl (Suprapur, Merck®), 65–69 % w/w HNO_3 (Analpure, Analityka®), ascorbic acid (analytical grade, Sigma-Aldrich®), KI (Suprapur, Merck®) and $NaBH_4$ (99.99 % trace metal basis, Sigma-Aldrich®) were used for sample preparation for Sb concentration and isotope analyses. Ethylenediaminetetraacetic acid disodium salt (EDTA, analytical grade, J. T. Baker®) and potassium hydrogen-phthalate (KHP, SigmaUltra, 99.95 %, Sigma-Aldrich) were used to prepare the eluent for Sb speciation analysis. Acetic acid (Suprapur, Merck®) and EDTA (analytical grade, J. T. Baker®) were used as additive for preserving Sb redox species in samples during Sb redox speciation analysis. Stock solutions of Sb(V) and Sb(III) at 1 $g.L^{-1}$ were prepared separately by dissolving an appropriate amount of potassium hexahydroxoantimonate(V) ($KSb(OH)_6$, analytical grade, Merck®) and potassium antimony(III) oxide tartrate hemihydrates ($K(SbO)C_4H_4O_6.0.5H_2O$, Extrapure, Merck®) in ultrapure water. Antimony concentration in Sb(V) and Sb(III) stock solutions were checked by ICP-MS. These solutions were used for preparing calibration solutions for Sb speciation analysis (separate calibration solutions for Sb(V) and Sb(III)) and for adsorption experiments. It is noteworthy that Sb(III) standard solution contained a small proportion of Sb(V). Therefore, Sb(V) was quantified in Sb(III) calibration standard solutions to correct Sb(III) concentrations of the calibration curve. In addition, it should be noted that Sb(III) adsorption experiments also contained ~2 % of Sb(V) at the beginning. This was taken into account in verifying the absence of oxidation during sorption experiments with Sb(III). The mono-elemental Sb SPEX standard solution (1000 µg mL^{-1} in 20 % w/w HCl, batch number 24-175SBX, SPEX CertiPrep) was used as Sb isotopic standard (Ferrari *et al.*, 2021).

All experiments were carried out in a lab with controlled temperature conditions (20 ± 1 °C). Sample dilutions and preparation for ICP-MS and HG-MC-ICP-MS analyses were carried out in class 10 000 cleanroom facility.

2.2. Ferrihydrite and schwertmannite synthesis and characterization

Two-line ferrihydrite was synthesized following the protocol of Schwertmann and Cornell (2000) and schwertmannite was synthesized following the protocol of Liu *et al.*, (2015) adapted from Regenspurg *et al.,* (2004). Details of the procedures are given in Appendix (Section 1). The quality of the synthetized ferrihydrite and schwertmannite was checked using XRD (X-ray powder diffraction), BET (Brunauer-Emmett-Teller) and SEM (Scanning Electron Microscopy, schwertmannite only) analysis (PAC and MEA platforms, Université de Montpellier). The methods and results are briefly presented in Appendix (Section 1, Figure A1 and A2).

2.3. Sorption experiments

Sorption experiments were conducted at different pH and initial Fe:Sb ratios. Every condition was made in duplicate or triplicate to check the reproducibility of the experiment. Intermediate suspensions of ferrihydrite or schwertmannite were prepared at 1 $g.L^{-1}$ and agitated for 48 h before the experiment to ensure homogeneity. Then, suspensions (50 mL) containing 0.01 $g.L^{-1}$ of ferrihydrite or schwertmannite in a 0.01 M $NaNO_3$ electrolyte were prepared in HDPE bottles and after a pH adjustment step, the suspensions were doped with Sb(III) or Sb(V) to reach a final Sb concentration of 0.1, 0.5, 1 and 10 $mg.L^{-1}$. As a result, the initial Fe:Sb molar ratios were 144, 29, 14 and 1.4 for Sb(III) adsorption experiment on ferrihydrite, 126, 25, 13 and 1.3 for Sb(V) adsorption experiment on ferrihydrite and 120, 24, 12 and 1.2 for Sb(III) and Sb(V) adsorption experiments on schwertmannite. In addition, procedural blanks containing ferrihydrite or schwertmannite were prepared and treated as samples to ensure that no contamination occurred at any step of the experiment. Finally, bottles were wrapped in an aluminium sheet and agitated at 300 rpm on a stirring table for 48 h at 20 ± 1 °C.

The pH of the suspensions was adjusted to correspond to the stability domain of ferrihydrite and schwertmannite observed in natural waters impacted by mine drainage (Bigham *et al.*, 1996). The pH was thus fixed at 6, 7 and 8 for ferrihydrite and 2.5 and 4.5 for schwertmannite using 0.1 M NaOH and 0.1 M HCl, respectively. The pH was monitored twice a day and re-adjusted when needed.

Sacrifices of the suspensions were carried out after 48 h, after chemical and isotopic equilibrium had been reached. This equilibrium time was defined based on preliminary kinetic monitoring for Sb(V) sorption on ferrihydrite and for Sb(III) and Sb(V) sorption on schwertmannite (Appendix, Table A1, Figure A3). Chemical equilibrium was reached in less than 48 h for all tested conditions and both minerals. These results were consistent with the literature regarding Sb sorption on ferrihydrite under conditions similar to the present study (initial Fe:Sb ratio = 100 , pH 7, in Qi and Pichler, (2016)) and Sb(V) sorption on schwertmannite which was reached in 24 h (Shan *et al.*, 2023). As concentration and isotopic equilibrium time may differ (Komárek *et al.*, 2021), it was also checked that isotopic equilibrium was reached after 48 h (Table A1, Figure A3). The results showed no significant difference in Sb isotope composition between 48 h and 96 h for all conditions (Table A1, Figure A3), which confirmed isotopic equilibrium achievement at 48 h.

Suspensions were filtered under vacuum using a Nalgene filtration unit and 0.22 µm pre-cleaned PVDF filters without rinsing step to avoid any bias related to Sb desorption from the mineral surfaces in line with other studies (e.g., Wasylenki et al., 2015; Gueguen et al., 2018; Zhou et al., 2022, 2023). Air was allowed to pass through the filter for a few minutes at the end of the filtration to ensure a complete separation of the dissolved and particulate phases. The filters were dried in a vacuum desiccator. An aliquot (10 mL) of the filtrate was acidified at 1 ‰ HNO_3 for dissolved Sb and Fe concentration measurement by ICP-MS (Inductively Coupled Plasma Mass Spectrometry). Another aliquot was acidified at 1 % HCl for Sb isotope ratio analysis by HG-MC-ICP-MS (Hydride Generation Multi-Collection Inductively Coupled Plasma Mass Spectrometry). A third aliquot was either analysed the same day for redox Sb speciation or preserved in 20 mM EDTA and 87 mM acetic acid and stored at 4 °C until analysis (< 1 week) as this combination of acids allow to stabilise Sb(III) (Wu and Pichler, 2016). The particulate phase collected on the filter was fully dissolved by placing the filter in a PTFE vial with 15 mL of 6 M HCl at 80 °C for 1 h (Schwertmann and Cornell, 2000) for subsequent Sb isotope analysis of the adsorbed Sb.

Sorption isotherms models were calculated using Freundlich and Langmuir isotherms as detailed in Appendix (Section 2, Equations A1 to A5).

2.4. Analytical methods

All analyses (ICP-MS, IC-ICP-MS, HG-MC-ICP-MS) were performed on the AETE-ISO platform (OSU OREME, Université de Montpellier) using routine protocols.

Antimony and iron concentrations in the dissolved (<0.22µm) and adsorbed (>0.22µm) fractions were measured by ICP-MS (Inductively Coupled Plasma Mass Spectrometry, iCAP TQ, ThermoScientific®) after an adequate dilution in 0.15 M HNO_3 (Ferrari *et al.*, 2021). Dissolved Fe was below quantification limits in filtrated samples representing less than 1 % of particulate Fe (except for two samples for which 4 % of total iron was in the dissolved fraction), showing that i) there was no significant dissolution of ferrihydrite or schwertmannite during the experiment and ii) colloidal ferrihydrite/schwertmannite was not present in the dissolved fraction (< 0.22 µm).

Antimony redox speciation analysis (Sb(V) and Sb(III) concentrations) was carried out by IC-ICP-MS (Ionic Chromatography coupled to ICP-MS, iCAP-Q, ThermoScientific®) using external Sb(III) and Sb(V) calibration. Chromatographic separation was performed using a Hamilton PRP-X100 column (15 cm x 4.6 mm i.d.) and precolumn (2 cm x 4.6 mm i.d.) with a Dionex ICS-5000 Ion Chromatography System (ThermoScientific®). A solution of 5 mmol.L^{-1} EDTA and 2 mmol.L^{-1} KHP (pH 4.5) was used as eluent with a flow rate of 1.5 mL.min^{-1}. A solution of indium at 1 µg.L^{-1} was continuously injected after the chromatographic separation and used as internal standard to correct potential sensitivity drifts of ICP-MS (Resongles *et al.*, 2013).

Antimony isotope composition was determined by HG-MC-ICP-MS (Hydride Generation coupled with a Multi-Collector ICP-MS, Neptune Plus, ThermoScientific®) as described in Ferrari *et al.*, (2021). HG-MC-ICP-MS configuration and parameters have been adapted to improve signal stability and the new settings are reported in Table A2. Antimony isotope composition was measured using a sample-standard bracketing method and is reported in the δ^{123}Sb notation (Equation 1).

$$\delta^{123}Sb(‰) = \left(\frac{\left(\frac{^{123}Sb}{^{121}Sb}\right)_{sample} - \left(\frac{^{123}Sb}{^{121}Sb}\right)_{mean\ std}}{\left(\frac{^{123}Sb}{^{121}Sb}\right)_{mean\ std}}\right) \times 1000 \quad \text{(Eq. 1)}$$

δ^{123}Sb of the dissolved and adsorbed fractions were measured after diluting the samples to 2 µg.L^{-1} of Sb in a 3 M HCl with 0.5 % w/v KI/ascorbic acid medium to ensure a full reduction of Sb(V) to Sb(III) as required for an optimal hydride generation (Ferrari *et al.*, 2021). Each sample was measured three times, at different times in the course of analytical sessions; the results reported in Table 1 correspond to the average and standard deviation of the three measurements. The preliminary Sb purification step described in Ferrari et al. (2021) was not required in the present study due to the low Fe:Sb ratios (<150) and the absence of interfering

elements (e.g., Se, As, Te, Sn) in the experimental samples (< detection limits). Furthermore, no shift of Sb isotope composition was observed between the Sb SPEX doped in experimental matrices (0.01 M $NaNO_3$ solution or ferrihydrite/schwertmannite dissolution solution in 6 M HCl) and the pure Sb SPEX standard solution ($\delta^{123}Sb$ = -0.00 ± 0.06 ‰ for Sb SPEX in $NaNO_3$ solution and $\delta^{123}Sb$ = -0.02 ± 0.02 ‰ in Fe/HCl solution).

$\delta^{123}Sb$ values of the stock solutions of Sb(III) and Sb(V) used in adsorption experiments were measured (n=3) at 0.32 ± 0.02 ‰ and 0.13 ± 0.05 ‰, respectively. Finally, different purified international certified reference materials (Sb recovery > 95 %) were measured (n=3, ±2σ) during every analytical session to ensure the accuracy of the analysis. They included sediments GSD-3 (0.14 ± 0.03 ‰), copper ore GXR-4 (0.39 ± 0.01 ‰), fly ash BCR 176R (-0.07 ± 0.02 ‰) and road dust BCR 723a (0.05 ± 0.06 ‰) and results were within the error of published $\delta^{123}Sb$ values (Ferrari et al., 2021). The $\delta^{123}Sb$ estimated from the repeated measurement of the Sb SPEX solution over all analytical sessions was 0.00±0.07 ‰ (2SD, n=201) which is consistent with the long-term precision published for the method in Ferrari et al. (2021).

3. RESULTS

3.1. Antimony sorption behaviour

The complete dataset of Sb(V) and Sb(III) adsorption experiments on ferrihydrite and schwertmannite are given in Table 1 and 2, respectively. Adsorption of Sb(III) and Sb(V) on ferrihydrite and schwertmannite was better described by Freundlich rather than Langmuir isotherm models ($0.89 < R^2 < 0.99$, Figure A4) as previously observed for Sb(III) and Sb(V) adsorption on ferrihydrite (Qi and Pichler, 2017; Zhou et al., 2023) and Sb(V) adsorption on schwertmannite (Shan et al., 2023) suggesting that the surface sites are heterogeneous and the adsorption multi-layered. Adsorption of Sb(V) on ferrihydrite decreased from pH 6 to 8 while adsorption of Sb(III) was not affected in this pH range (except at low Fe:Sb ratio = 1), in agreement with previous studies (Guo et al., 2014; Qi and Pichler, 2017; Zhou et al., 2023). The amount of Sb(V) adsorbed on ferrihydrite (5 to 208 mg/g) was comparable to the values measured in Zhou et al. (2023) with a similar pH, Fe:Sb ratio and ferrihydrite properties. In terms of Sb surface coverage, adsorption capacity of ferrihydrite at pH 6 was similar for Sb(III) and Sb(V), with values from 23 µg/m² and 24 µg/m² for a high molar ratio Fe:Sb of 127, to 529 ± 45 µg/m² and 499 µg/m² for a low Fe:Sb ratio of 1, respectively. Adsorption of Sb(V) on schwertmannite was similar at pH 2.5 and 4.5 while adsorption of Sb(III) increased at pH 4.5 compared to pH 2.5. Schwertmannite presented a higher Sb surface coverage than ferrihydrite, for example for a Fe:Sb ratio of 1 at pH 4.5, Sb(III) and Sb(V) surface coverage were 2320 and 2289 µg/m², respectively (Table 2). The sorption capacity of Sb(V) was for the lowest Fe:Sb(V) ratio at pH 2.5 was 160-205 mg/g, in the same order of magnitude of the value of 253 mg/g found by Shan et al. (2023) in similar conditions (pH=3, Fe:Sb ratio of 2.5).

For Sb(III) adsorption experiments, dissolved Sb speciation was measured at the end of the experiments (t= 48 h). Final Sb(V) concentration was comprised between 3 µg/L (for initial Sb concentration of 100 µg/L) and 197 µg/l (for initial Sb concentrations of 10000 µg/L) (Table 1 and 2). This was similar or even lower than initial dissolved Sb(V) concentration brought by Sb(V) contamination from the Sb(III) standard solution. Slight excess of Sb(V) was noted in ferrihydrite sorption experiments at pH 8 and high Fe:Sb ratios; however, it represented a maximum of 9 % of total initial Sb. Considering the preferential adsorption of Sb(III) over Sb(V) in competitive scenarios (Qi and Pichler, 2016, 2017), the persistence of Sb(III) as the dominant species (> 90 % after 48 h) in the dissolved fraction during Sb(III)

adsorption experiments suggests minimal Sb(III) oxidation. Furthermore, according to our previous experimental and theoretical investigations (Ferrari et al., 2022, 2023), abiotic Sb(III) oxidation was expected to decrease the $\delta^{123}Sb$ value of remaining dissolved Sb(III), which was opposed to observations made in the present experiments. This is also coherent with the conclusions of Guo et al. (2014) who noted that the rapid oxidation of Sb(III) to Sb(V) due to the oxidative reactivity of Fe(III) during its adsorption is highly improbable.

314 **Table 1.** All experimental data of Sb(V) and Sb(III) adsorption experiments on ferrihydrite.

Samples	pH		Fe:Sb initial molar ratio	Total dissolved Sb (µg/L)		Dissolved Sb redox speciation (µg/L)			Adsorbed Sb at equilibrium (t=48 h) (%)	Surface coverage at equilibrium		Isotope composition of the dissolved fraction (t=48 h)		Isotope composition of the adsorbed fraction (t=48 h)		$\Delta^{123}Sb_{solid-solution}$ (‰)
	Average	σ		Initial (t=0 h)	Final at equilibrium (t=48 h)*	Sb(V) initial (t=0 h)**	Sb(III) final (t=48 h)***	Sb(V) final (t=48 h)***		µg Sb/m²	mg Sb/g	δ^{123}Sb (‰) Average	δ^{123}Sb (‰) 2σ	δ^{123}Sb (‰) Average	δ^{123}Sb (‰) 2σ	
Sb(V)-ferrihydrite																
Sb(V) stock solution	n.a.	n.a.	n.a.	n.a.	n.a.	n.a.	n.a.	n.a.	n.a.	n.a.	n.a.	0.13	0.05	n.a.	n.a.	n.a.
Sb(V)_0.1ppm-pH 6	5.9	0.1	127	100	14	n.a.	n.a.	n.a.	86	23	9	0.51	0.05	0.16	0.10	-0.35
Sb(V)_0.5ppm-pH 6	6.0	0.1	25	500	130	n.a.	n.a.	n.a.	74	99	37	0.53	0.05	0.08	0.04	-0.45
Sb(V)_1ppm-pH 6	6.0	0.0	13	999	413	n.a.	n.a.	n.a.	59	158	59	0.39	0.05	-0.07	0.14	-0.46
Sb(V)_10ppm-pH 6_1	6.3	0.1	1	9990	7911	n.a.	n.a.	n.a.	21	559	208	0.26	0.06	-0.11	0.10	-0.37
Sb(V)_10ppm-pH 6_2	6.1	0.1	1	9990	8213	n.a.	n.a.	n.a.	18	478	178	0.16	0.02	-0.15	0.04	-0.31
Sb(V)_10ppm-pH 6_3	6.1	0.1	1	9990	7941	n.a.	n.a.	n.a.	21	551	205	0.10	0.11	-0.1	0.02	-0.20
Sb(V)_0.1ppm-pH 7	7.0	0.1	127	100	42	n.a.	n.a.	n.a.	58	16	6	0.39	0.02	-0.05	0.04	-0.44
Sb(V)_0.5ppm-pH 7	7.1	0.2	25	500	274	n.a.	n.a.	n.a.	45	61	23	0.28	0.06	-0.12	0.06	-0.40
Sb(V)_1ppm-pH 7	7.1	0.2	13	999	528	n.a.	n.a.	n.a.	47	127	47	0.24	0.03	-0.05	0.04	-0.29
Sb(V)_10ppm-pH 7	7.1	0.1	1	9990	8812	n.a.	n.a.	n.a.	12	317	118	0.14	0.02	-0.15	0.05	-0.29
Sb(V)_0.1ppm-pH 8	8.0	0.6	127	100	53	n.a.	n.a.	n.a.	47	13	5	0.29	0.03	0	0.09	-0.29
Sb(V)_0.5ppm-pH 8	7.9	0.6	25	500	323	n.a.	n.a.	n.a.	35	47	18	0.27	0.01	-0.11	0.10	-0.38
Sb(V)_1ppm-pH 8	8.0	0.5	13	999	585	n.a.	n.a.	n.a.	41	111	41	0.23	0.05	-0.14	0.02	-0.37
Sb(V)_10ppm-pH 8	7.9	0.5	1	9990	8440	n.a.	n.a.	n.a.	16	417	155	0.16	0.06	-0.19	0.02	-0.34
Sb(III)-ferrihydrite																
Sb(III) stock soluton	n.a.	n.a.	n.a.	n.a.	n.a.	n.a.	n.a.	n.a.	n.a.	n.a.	n.a.	0.32	0.02	n.a.	n.a.	n.a.
Sb(III)_0.1ppm-pH 6	6.0	0.1	144	108	40	2	37	4	62	24	7	0.63	0.07	0.23	0.08	-0.40
Sb(III)_0.5ppm-pH 6	5.9	0.1	29	483	264	9	271	6	42	73	21	0.51	0.06	0.22	0.06	-0.29
Sb(III)_1ppm-pH 6	5.9	0.1	14	1072	n.d.	20	625	9	41	155	44	0.46	0.03	0.15	0.04	-0.31
Sb(III)_10ppm-pH 6	5.9	0.0	1	10626	n.d.	202	9172	48	13	499	141	0.36	0.05	0.25	0.06	-0.11
Sb(III)_0.1ppm-pH 7	7.0	0.2	144	108	n.d.	2	41	3	60	23	6	0.53	0.05	0.30	0.06	-0.24
Sb(III)_0.5ppm-pH 7	6.8	0.1	29	483	n.d.	9	206	13	54	93	26	0.51	0.05	0.24	0.03	-0.27
Sb(III)_1ppm-pH 7	6.9	0.1	14	1072	638	20	640	18	39	147	41	0.46	0.05	0.24	0.05	-0.22
Sb(III)_10ppm-pH 7	6.8	0.1	1	10626	7978	202	9267	38	12	468	132	0.38	0.08	0.07	0.05	-0.30
Sb(III)_0.1ppm-pH 8[Ŧ]	8.1	0.4	144	108	n.d.	2	17	10	74	28	8	0.46	0.07	0.33	0.03	-0.13
Sb(III)_0.5ppm-pH 8	8.1	0.4	29	483	188	9	189	29	55	94	26	0.53	0.02	0.25	0.03	-0.28
Sb(III)_1ppm-pH 8	8.1	0.4	14	1072	n.d.	20	653	41	35	134	38	0.47	0.03	0.18	0.05	-0.29
Sb(III)_10ppm-pH 8	8.1	0.4	1	10626	n.d.	202	9535	130	9	341	96	0.36	0.02	0.19	0.06	-0.17

n.a. not applicable

n.d. not determined

*Total Sb concentration determined by ICP-MS

**Sb(V) concentration corresponding to 1.9% of initial Sb

***Sb(III) and Sb(V) concentrations measured by IC-ICP-MS

[Ŧ]Filtration joint failure occurred during the filtration of the sample, some particles likely have been recovered in the dissolved fraction (< 0.22µm).

315 **Table 2.** All experimental data of Sb(V) and Sb(III) adsorption experiments on schwertmannite.

Samples	pH		Fe:Sb initial molar ratio	Total dissolved Sb (µg/L)		Dissolved Sb redox speciation (µg/L)			Adsorbed Sb at equilibrium (t=48 h) (%)	Surface coverage at equilibrium		Isotope composition of the dissolved fraction (t=48 h)		Isotope composition of the adsorbed fraction (t=48 h)		$\Delta^{123}Sb_{solid-solution}$ (‰)
	Average	σ		Initial (t=0 h)	Final at equilibrium (t=48 h)*	Sb(V) initial (t=0 h)**	Sb(III) final (t=48 h)***	Sb(V) final (t=48 h)***		µg Sb/m²	mg Sb/g	δ^{123}Sb (‰) Average	δ^{123}Sb (‰) 2σ	δ^{123}Sb (‰) Average	δ^{123}Sb (‰) 2σ	
Sb(V)-schwertmannite																
Sb(V)_0.1ppm-pH 2.5	2.6	0.0	120	112	26	n.a.	n.a.	n.a.	76	171	9	0.35	0.02	0.07	0.03	-0.28
Sb(V)_0.5ppm-pH 2.5	2.6	0.0	24	475	210	n.a.	n.a.	n.a.	56	529	26	0.31	0.04	0.01	0.05	-0.30
Sb(V)_1ppm-pH 2.5	2.6	0.2	12	1179	451	n.a.	n.a.	n.a.	62	1455	73	0.29	0.07	-0.01	0.09	-0.30
Sb(V)_10ppm-pH 2.5_1	2.6	0.0	1.2	9990	8393	n.a.	n.a.	n.a.	16	3195	160	0.16	0.02	-0.10	0.07	-0.26
Sb(V)_10ppm-pH 2.5_2	2.6	0.1	1	9990	7936	n.a.	n.a.	n.a.	21	4110	205	0.15	0.04	-0.08	0.06	-0.23
Sb(V)_0.1ppm-pH 4.5	4.6	0.0	120	112	6	n.a.	n.a.	n.a.	95	212	11	0.42	0.04	0.13	0.06	-0.29
Sb(V)_0.5ppm-pH 4.5	4.6	0.0	24	475	106	n.a.	n.a.	n.a.	78	738	37	0.43	0.03	0.11	0.07	-0.31
Sb(V)_1ppm-pH 4.5	4.6	0.0	12	1179	410	n.a.	n.a.	n.a.	65	1537	77	0.31	0.04	0.03	0.06	-0.28
Sb(V)_10ppm-pH 4.5_1	4.6	0.1	1	9990	8831	n.a.	n.a.	n.a.	12	2320	116	0.17	0.03	-0.05	0.07	-0.21
Sb(V)_10ppm-pH 4.5_2	4.6	0.1	1	9990	9544	n.a.	n.a.	n.a.	4	894	45	0.17	0.02	-0.06	0.02	-0.23
Sb(III)-schwertmannite																
Sb(III)_0.1ppm-pH 2.5	2.6	0.0	120	107	38	2	28	2	65	140	7	0.66	0.04	0.20	0.05	-0.46
Sb(III)_0.5ppm-pH 2.5	2.6	0.1	24	527	254	10	202	7	52	546	27	0.53	0.02	0.14	0.03	-0.39
Sb(III)_1ppm-pH 2.5	2.6	0.1	12	1058	708	20	630	15	33	699	35	0.48	0.04	0.09	0.05	-0.39
Sb(III)_10ppm-pH 2.5	2.6	0.1	1	9991	9281	190	9204	178	7	1421	71	0.34	0.03	0.02	0.07	-0.32
Sb(III)_0.1ppm-pH 4.5	4.6	0.0	120	107	12	2	7	3	89	190	10	0.68	0.01	0.35	0.05	-0.33
Sb(III)_0.5ppm-pH 4.5	4.5	0.0	24	527	114	10	108	4	78	826	41	0.62	0.08	0.28	0.03	-0.34
Sb(III)_1ppm-pH 4.5	4.5	0.1	12	1058	385	20	341	32	64	1345	67	0.59	0.06	0.22	0.06	-0.37
Sb(III)_10ppm-pH 4.5	4.4	0.1	1	9991	8846	190	8478	197	11	2289	114	0.38	0.07	0.12	0.04	-0.26

n.a. not applicable

n.d. not determined

*Total Sb concentration determined by ICP-MS

**Sb(V) concentration corresponding to 1.9% of initial Sb

***Sb(III) and Sb(V) concentrations measured by IC-ICP-MS

3.2. Antimony isotope fractionation

3.2.1 Isotope fractionation during Sb adsorption on ferrihydrite

There was a significant isotope fractionation of Sb between the dissolved and adsorbed phases. The isotope fractionation during adsorption of Sb(V) and Sb(III) on ferrihydrite followed a closed-system equilibrium fractionation model (R^2 = 0.87 for dissolved Sb(V) experimental vs modelled values and R^2= 0.64 for Sb(III), Figure A5), with a parallel increase of the isotopic signature of the dissolved and adsorbed phases (Figure 1). The fractionation factor $\Delta^{123}Sb_{solid\text{-}solution}$ averaged -0.34 ± 0.08 ‰ for Sb(V) and -0.25 ± 0.08 ‰ for Sb(III), with the dissolved phase preferentially enriched in the heavy isotope (^{123}Sb), for both Sb(III) and Sb(V) species. Under the experimental conditions, pH and Sb surface coverage did not influence the magnitude of $\Delta^{123}Sb_{solid\text{-}solution}$ fractionation factor (Figure 2a-c). Only one data from Sb(III) sorption experiments deviated from the general trend for the dissolved phase in Figure 1b; it was the sample with 74 % adsorption at pH 8, for which a failure of the filter joint occurred during the filtration most likely causing the release of some particles into the dissolved fraction and explaining the lower $\Delta^{123}Sb_{solid\text{-}solution}$ observed (this is also supported

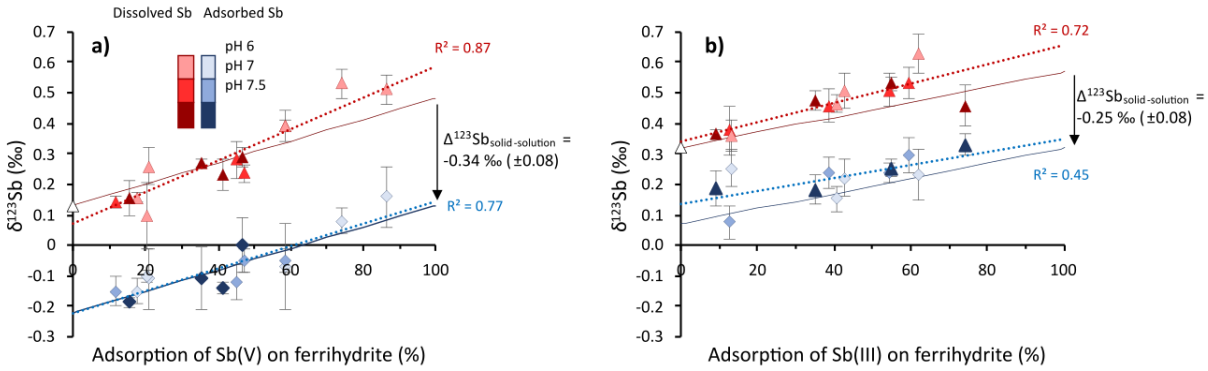

by the presence of 4 % of initial solid Fe in solution at equilibrium).

Figure 1. Antimony isotope composition ($\delta^{123}Sb$) of dissolved (red) and adsorbed (blue) phases during (a) Sb(V) and (b) Sb(III) adsorption on ferrihydrite. The white triangles represent the signature of starting Sb(III) or Sb(V) stock solutions. Dotted lines represent the regression lines for the entire dissolved (red) or adsorbed (blue) experimental dataset. Solid lines represent the theorical $\delta^{123}Sb$ of the dissolved (red) and adsorbed (blue) Sb using an equilibrium fractionation model and the average $\Delta^{123}Sb_{solid\text{-}solution}$ determined experimentally.

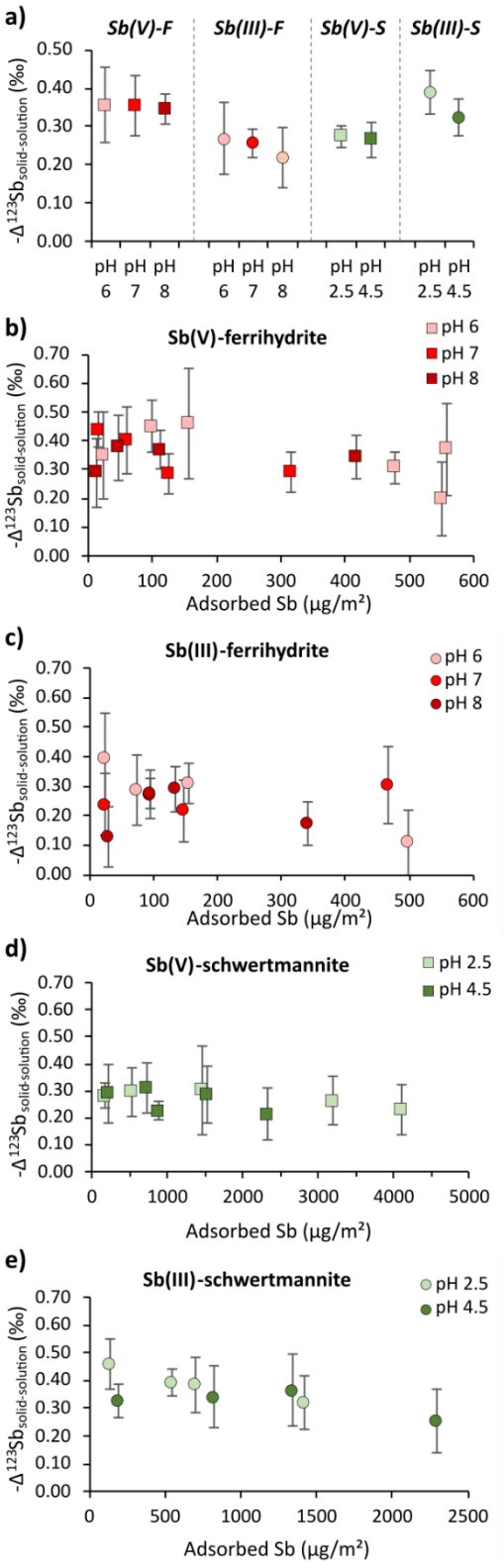

Figure 2. a) Average apparent fractionation factor between the solution and the solid phase ($-\Delta^{123}Sb_{solid\text{-}solution}$) calculated at pH 6, 7 and 8 for Sb(V) (Sb(V)-F) and Sb(III) (Sb(III)-F) adsorption on ferrihydrite and at pH 2.5 and 4.5 for Sb(V) (Sb(V)-S) and Sb(III) (Sb(III)-S) adsorption on schwertmannite. Figures 2b to 2e represent the average apparent fractionation factor ($-\Delta^{123}Sb_{solid\text{-}solution}$) as a function of Sb surface coverage (µg/m²) during adsorption of b) Sb(V) on ferrihydrite, c) Sb(III) on ferrihydrite, d) Sb(V) on schwertmannite and e) Sb(III) on schwertmannite. On Figures 2b to 2e, the error bars correspond to the propagation of the analytical error on the measurement of dissolved and adsorbed isotopic composition ($\delta^{123}Sb$).

3.2.2 Isotope fractionation during Sb adsorption on schwertmannite

The fractionation of $\delta^{123}Sb$ was also significant between the dissolved and adsorbed phases during Sb adsorption on schwertmannite. As for the adsorption of Sb species on ferrihydrite, the adsorption of Sb(V) and Sb(III) on schwertmannite followed a closed system equilibrium fractionation model (Figure 3, Figure A5 : $R^2 = 0.94$ for dissolved Sb(V) and Sb(III) between modelled and experimental data). The fractionation factor $\Delta^{123}Sb_{solid\text{-}solution}$ averaged -0.36 ± 0.06 ‰ for Sb(III) and -0.27 ± 0.03 ‰ for Sb(V), with the dissolved phase preferentially enriched in the heavy isotope (^{123}Sb). Neither the pH nor the surface coverage significantly influenced Sb isotope fractionation within the range experimental conditions (Figure 2a, d and e).

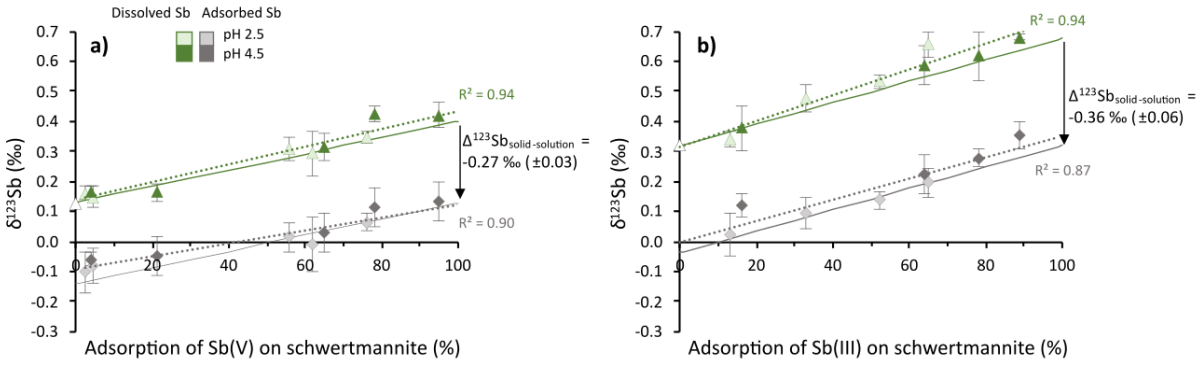

Figure 3. Antimony isotope composition ($\delta^{123}Sb$) of dissolved (green) and adsorbed (grey) phases during (a) Sb(V) and (b) Sb(III) adsorption on schwertmannite. The white triangles represent the signature of starting Sb(III) or Sb(V) stock solutions. Dotted lines represent the regression lines for the entire dissolved (green) or adsorbed (grey) experimental dataset. Solid lines represent the theorical $\delta^{123}Sb$ of the dissolved (green) and adsorbed (grey) Sb using an equilibrium fractionation model and the average $\Delta^{123}Sb_{solid\text{-}solution}$ determined experimentally.

4. DISCUSSION

4.1. Antimony isotope fractionation during its adsorption of ferrihydrite

Only a few other studies investigated the fractionation of antimony isotopes on iron- (Araki et al., 2009; Zhou et al., 2023) or aluminium- (Zhou *et al.*, 2022) oxyhydroxides and these studies focused only on the sorption of Sb(V) species. Zhou *et al.* (2022) showed that although kinetic fractionation occurs at the early stage of the reaction, Sb(V) adsorption on aluminium oxides does not produce significant equilibrium Sb isotope fractionation and explained the lack of fractionation by the formation of an outer-sphere complex of Sb on γ-Al_2O_3, with similar bond length of Sb - O (~ 1.98 Å) and octahedral bond structure of $Sb(OH)_6^-$ in the aqueous and solid phases (Zhou et al., 2022). On the other hand, our study shows a preferential adsorption of the light ^{121}Sb(III) and ^{121}Sb(V) isotope onto ferrihydrite and schwertmannite, with a fractionation factor $\Delta^{123}Sb_{solid\text{-}solution}$ around -0.3 ‰. This value is similar, yet slightly lower, to the equilibrium fractionation factor ($\Delta^{123}Sb_{solid\text{-}solution}$ of -0.49 ‰) measured by Zhou et al. (2023) for Sb(V) adsorption on ferrihydrite while antimony(V) adsorption on hematite and goethite generated higher fractionation ($\Delta^{123}Sb_{solid\text{-}solution}$ = -1.12 ± 0.01 ‰ for hematite and -1.14 ± 0.05 ‰ for goethite).

For the sorption of Sb(V) on ferrihydrite, sorption mechanisms and local structures of adsorbed-Sb(V) can be obtained from previous sorption studies carried out in similar conditions. In the study of Araki *et al.* (2009) and Zhou et al. (2023) which both evidenced slight enrichment in the heavy isotope in the aqueous phase compared to Sb(V) adsorbed on ferrihydrite, Sb(V) was present as an inner-sphere complex of octahedral Sb species on the ferrihydrite surface (Mitsunobu *et al.,* 2006; Zhou et al., 2023). Thus, the octahedral bond structure of Sb(V) was the same in the aqueous ($Sb(OH)_6^-$) and adsorbed Sb(V). There was no change in the first coordination shell between aqueous and adsorbed Sb(V) both in terms of coordination number and Sb(V)–O bond lengths of ~ 1.97-1.98 Å (Mitsunobu et al., 2010; Tella and Pokrovsky, 2012; Zhou et al., 2023). The sorption process involved the formation of Sb – O – Fe bonds with an edge-sharing and corner-sharing configurations (Scheinost *et al.*, 2006; McComb *et al.,* 2007, Guo et al., 2014). This was confirmed by Mitsunobu *et al.* (2010) who also demonstrated the double corner-sharing complex character of the inner-sphere formation and more recently by Zhou et al. (2023). One could have expected that this mode of complexation would generate no fractionation or slight enrichment in the heavy isotope in the adsorbed Sb(V) species (stronger bonding due to inner-sphere complexation), while the

reverse was observed. Nickel adsorption onto various Fe oxyhydroxides through inner-sphere complexes also showed lighter Ni isotope enrichment in the adsorbed fraction on ferrihydrite ($\Delta^{60/58}Ni_{solid\text{-}solution}$ value of -0.35 ± 0.10 ‰ for Ni on ferrihydrite, (Wasylenki *et al.*, 2015; Wang and Wasylenki, 2017; Gueguen *et al.*, 2018)). Considering that Ni - O bonds in the adsorbed complexes were not significantly longer and weaker (therefore, Ni bonding was not weaker) than in the predominant aqueous species, the authors ascribed this fractionation direction to distortions of bond angles and lengths occurring in the adsorbed complexes NiO_6 (Wasylenki *et al.*, 2015). More recently, Yan *et al.* (2021) observed the same effect for Cd; fractionation of Cd isotopes during sorption onto Fe oxyhydroxides and enrichment in the light isotopes in the solid were attributed to distortion of the CdO_6 complexes during adsorption (Yan *et al.*, 2021). For antimony, our theoretical calculations using the Density Functional Theory suggested that the appearance in the structure of a second neighbour other than the Sb species induced a slight distortion of the atomic polyhedron (both on Sb – O bond lengths and on the O – Sb – O angle) susceptible to cause isotopic fractionation of around 0.3 ‰, in the same order of magnitude as measured in this study (Ferrari *et al.,* 2022). In the present study, the atomic distortion induced by iron as the second closest neighbour may be the cause of the slight enrichment in lighter Sb isotopes in the solid. Regarding the possible effect of surface coverage on the isotope fractionation during sorption (evidenced for example for Zn adsorption onto Mn oxyhydroxide, Bryan *et al.*, 2015), our data showed no influence, within a range of Fe:Sb molar ratios of 1.4 - 144 (Sb(III)) and 1.3 – 126 (Sb(V)). This was in agreement with the results of Mitsunobu *et al.* (2010) and Zhou et al. (2023) who showed that there was no change in the local structures of Sb species in Sb(V)-adsorbed ferrihydrite at various Fe:Sb ratios (20-1000).

pH has an important effect on the sorption of metals and metalloids onto Fe-oxyhydroxides because it influences both the surface charge of the solid (thus, the surface coverage) and the aqueous speciation of elements (thus the potential fractionation among the aqueous species and the possible different affinity of the different aqueous species for the solid). Therefore, pH changes may induce variations in metal isotope fractionation factors between adsorbed and aqueous species (for example for Zn, see references in Komárek *et al.* (2021); for Mo (Goldberg *et al.,* 2009) ; or for Se (Xu *et al.*, 2020)). Here, Sb(V) sorption on ferrihydrite was higher at pH 6 than at pH 7 – 8. The point of zero charge (pzc) of synthetic Fe-oxides usually ranges between pH 7 and 9 (Parks, 1965; Schwertmann and Cornell, 2000), which suggests that the surface charge of ferrihydrite in the present sorption experiments could be slightly more positive at pH 6 than at pH 7 - 8. Regarding Sb speciation in solution, Sb(V) species

belongs to the acid/base couple $Sb(OH)_5/Sb(OH)_6^-$, with a pKa value of 2.848 (25 °C) (Accornero *et al.,* 2008); thus, Sb(V) is in the form of anionic $Sb(OH)_6^-$ species in the whole pH range of sorption experiments on ferrihydrite (pH 6 – 8) (Filella et al., 2002). Therefore, the higher Sb(V) sorption on ferrihydrite at pH 6 could be related to the slight change of ferrihydrite surface charge. However, this change did not significantly affect Sb isotope fractionation amplitude. A similar result was obtained for selenium; although pH influenced the amount of Se(IV) adsorbed on hematite, it did not significantly change Se isotopic fractionation (Xu *et al.*, 2020) and for Sb(V) adsorbed on ferrihydrite, hematite and goethite which did not show changes in complex structures with varying pH (Zhou et al., 2023).

Regarding Sb(III), aqueous speciation was not expected to change significantly over the whole pH range of ferrihydrite sorption experiments (6 – 8) (representing either 100% of uncharged $Sb(OH)_3$ over pH 6 – 8 (Filella et al., 2002) or > 85 % of anionic tartrate complex over pH 6 – 8 (Biver, 2021), depending if tartrate complexation is considered or not). This is consistent with the negligible effect of pH on sorption isotherms and Sb isotope fractionation between adsorbed and aqueous Sb observed in the present study. Antimony isotope fractionation resulting from the adsorption of Sb(III) on ferrihydrite was on average slightly lower than that of Sb(V) possibly due to slight differences in complexation configuration as observed among the different mineral phases (Zhou et al., 2022, 2023) but the difference remains small and would require an in-depth molecular speciation study to be further discussed.

4.2. Influence of the mineral nature

Metal isotope fractionation during their adsorption on minerals varies according to the mineralogy (Komárek *et al.*, 2021). Here, sorption experiments with schwertmannite were conducted at acid pH values (i.e., 2.5 – 4.5), corresponding to the stability domain of this mineral, which is different from that of ferrihydrite (i.e., 6 – 8); thus, the effects of mineral on Sb isotope fractionation during sorption cannot be distinguished from pH effect. Sorption studies of antimony on schwertmannite are rare in the literature. Nagano *et al.* (2011) showed that Sb oxyanions had a high affinity for natural schwertmannite found in AMD-impacted river and suggested the formation of inner-sphere complexes at the schwertmannite surface. Shan et al. (2023) recently revealed that Sb(V) is complexed on schwertmannite through the formation of edge-sharing and double corner-sharing complexes at the surface and the tunnel inner-surface of schwertmannite similarly to ferrihydrite. The proportion of surface species

was dependent on pH (in the pH range 3-9) and on Sb loading (in the Fe:Sb ratio range 2.5 – 250); at low Sb(V) loading and alkaline pH, Sb(V) sorption was also accompanied by the incorporation of Sb(V) in the mineral lattice (Shan et al. 2023). In the present study, Sb isotope fractionation was not significantly different between pH 2.5 and 4.5 probably because the proportion of Sb(V) surface species does not vary significantly in this pH range, in agreement with the surface complexation modelling calculations of Shan et al. (2023). The Sb surface coverage (Fe:Sb from 1.2 to 120) did not influence Sb isotope fractionation suggesting that Sb(V) incorporation in the Fe-O octahedron does not fractionate Sb isotopes or that the proportion of Sb(V) incorporated remains too limited to affect the apparent isotope fractionation.

Only one study, Li *et al.* (2016), investigated the sorption behaviour of Sb(III) and Sb(V) on schwertmannite separately, at different pH. Over the pH range 3.5 - 5.0, Sb(III) and Sb(V) are adsorbed efficiently (Li *et al.*, 2016). Our results corroborated these findings, with very similar maximum Sb sorption densities obtained for Sb(III) (2289 µg.m², i.e., 114 $mg.g^{-1}$) and for Sb(V) (2320 µg.m², i.e., 116 $mg.g^{-1}$) at pH 4.5. pH had little effect on the sorption of Sb(V) on schwertmannite ($Sb(OH)_6^-$ predominated over $Sb(OH)_5$ at pH 2.5 and 4.5 (Filella et al., 2002)) while Sb(III) sorption increased slightly at pH 4.5 compared to pH 2.5, which could be related to change in schwertmannite protonation (Li et al., 2016) rather than change in aqueous Sb(III) speciation (predominant Sb(III) species did not change at pH 2.5 and at pH 4.5, whether tartrate complexation is considered (Biver, 2021) or not (Filella et al., 2002) in the speciation calculation). Nevertheless, the slight change of reactivity of Sb(III) with pH had no significant effect on Sb isotope fractionation between adsorbed- and aqueous-Sb, and finally the amplitude and direction of Sb isotope fractionation factors with schwertmannite were similar to those obtained with ferrihydrite. In both cases, the isotope fractionation could arise from the distortion of the atomic polyhedron of Sb(III) and Sb(V) during sorption and the apparition of Fe-Sb in the second shell, which leads to small changes in bond lengths, angles and volume, and induces an increase of the disorder of the structure and thus weaker bonds favouring light isotopes. Such a mechanism has been suggested to explain isotope fractionation observed in several sorption studies for Ge (Pokrovsky *et al.*, 2014), Mo (Wasylenki *et al.*, 2011), Cd (Yan *et al.,* 2021) and Ni (Wasylenki *et al.*, 2015; Wang and Wasylenki, 2017; Gueguen *et al.*, 2018), and theoretical study for Sb (Ferrari *et al.*, 2022). Extended X-ray adsorption fine structure (EXAFS) measurements would be necessary to better characterise the local structure of Sb(III) species in ferrihydrite and schwertmannite.

4.3. Environmental significance

Schwertmannite and ferrihydrite are typical Sb-bearing phases in rivers impacted by AMD and the main control of Sb mobility. The experimental conditions (mineral phases, pH, initial concentration of Sb(V) and Sb(III), ionic strength) were designed to be relevant to natural waters impacted by AMD. Therefore, the relatively uniform fractionation factor $\Delta^{123}Sb_{solid\text{-}solution}$ around -0.3 ‰ obtained between adsorbed- and aqueous-Sb in the present study is of particular interest in the perspective of tracing sorption process in environmental studies. However, this value obtained in laboratory conditions with simple solution chemistry must be compared to apparent fractionation factors in real AMD-impacted streams whose chemistry is more complex than experimental conditions. A few data are available from the literature; a slight heavy Sb isotopic enrichment was observed in a drainage water sample from the Ichinokawa mine in Japan compared to the data from Sb minerals (Sb_2S_3) collected in the same area (Tanimizu *et al.*, 2011). The isotopic fractionation was ascribed to adsorption equilibrium with Fe hydroxides in the surrounding sediment. It was in line with the results of laboratory experiments of Sb(V) sorption on ferrihydrite which also indicated a slight enrichment of the heavier Sb isotope in the aqueous phase compared to adsorbed Sb (Araki *et al.,* 2009). In an ongoing study, Resongles *et al.* (2021) showed an apparent fractionation of -0.35‰ between river sediments and water in a stream impacted by AMD at the San José mine (Oruro, Bolivia), suggesting that adsorption may be an important process leading to an enrichment in heavy Sb isotope in AMD waters. These results tend to validate the fractionation factors obtained in the laboratory in the present study and show that Sb isotopes may be useful to investigate the mechanisms controlling Sb fate in mining-impacted rivers. However, recent studies also showed that biotic and abiotic redox changes generate Sb isotope fractionation with factors in the same order of magnitude as observed for adsorption indicating that Sb isotope signature in natural systems can result from a complex series of processes (Ferrari et al., 2023, Veldhuizen et al., 2023). Besides, molecular-scale studies showed that the incorporation of Sb(V) into the structure of schwertmannite by substitution of Fe(III) occurs at low Sb(V) loading and alkaline pH, stabilizing the schwertmannite over a larger range of pH (Rastegari et al., 2022, Shan et al., 2023), further study of the isotope fractionation associated with this process would be required.

5. CONCLUSION

This study showed that sorption on ferrihydrite and schwertmannite induced a slight enrichment in the light isotopes in adsorbed Sb, with no significant effect of pH, Fe:Sb ratio, or redox Sb species under the study conditions. The $\Delta^{123}Sb_{solid\text{-}solution}$ values obtained for sorption on ferrihydrite were -0.25 ± 0.08 ‰ for Sb(III) and -0.34 ± 0.08 ‰ for Sb(V). For sorption on schwertmannite, the $\Delta^{123}Sb_{solid\text{-}solution}$ values obtained were -0.36 ± 0.06 ‰ for Sb(III) and -0.27 ± 0.03 ‰ for Sb(V). The observed isotopic fractionation followed a closed system equilibrium model and could result from the distortion of the atomic polyhedron formed by Sb(III) and Sb(V) due to the appearance of iron as second closest Sb neighbour during the Sb adsorption, thus decreasing the polyhedral symmetry. This study gives new interpretation tools for the understanding of the isotopic cycle of Sb in mining and natural environments.

6. ACKNOWLEDGEMENTS

This work received financial support from the CNRS INSU EC2CO program (Project AntiBol), the French Research National Agency ANR (project ANTIMONY, grant number ANR-22-CE01-0016-01) and the Ecole Doctorale GAIA (PhD fellowship of Colin Ferrari, 2019-2022). We thank Sophie Delpoux and Léa Causse for the speciation and trace element analysis performed on the AETE-ISO platform, OSU OREME/Université de Montpellier and Laura Blanc, David Clousier and Léa Pradeilles for their help during the experiments. We would like to acknowledge Nicolas Donzel and Bernard Fraisse from the PAC platform and Frédéric Hernandez from the MEA platform, Université de Montpellier, for BET surface area measurement, DRX analysis and SEM images, respectively.

7. REFERENCES

Accornero, M., Marini, L. and Lelli, M. (2008) 'The Dissociation Constant of Antimonic Acid at 10–40 °C', *Journal of Solution Chemistry*, 37(6), pp. 785–800. https://doi.org/10.1007/s10953-008-9280-4.

Araki, Y., Tanimizu, M. and Takahashi, Y. (2009) 'Antimony isotopic fractionation during adsorption on ferrihydrite', *Geochimica et Cosmochimica Acta Supplement*, 73, p. A49.

Asaoka, S. *et al.* (2011) 'Preconcentration Method of Antimony Using Modified Thiol Cotton Fiber for Isotopic Analyses of Antimony in Natural Samples', *Analytical Sciences*, 27, pp. 25–28. https://doi.org/10.2116/analsci.27.25

Balistrieri, L.S. *et al.* (2008) 'Fractionation of Cu and Zn isotopes during adsorption onto amorphous Fe(III) oxyhydroxide: Experimental mixing of acid rock drainage and ambient river water', *Geochimica et Cosmochimica Acta*, 72(2), pp. 311–328. https://doi.org/10.1016/j.gca.2007.11.013.

Beauchemin, S. et al. (2012). Downstream changes in antimony and arsenic speciation in sediments at a mesothermal gold deposit in British Columbia, Canada. *Applied geochemistry*, *27*(10), pp. 1953-1965. https://doi.org/10.1016/j.apgeochem.2012.04.003.

Belzile, N., Chen, Y.-W. and Wang, Z. (2001) 'Oxidation of antimony (III) by amorphous iron and manganese oxyhydroxides', *Chemical Geology*, 174(4), pp. 379–387. https://doi.org/10.1016/S0009-2541(00)00287-4.

Bolan, N., et al. (2022) 'Antimony contamination and its risk management in complex environmental settings: a review.' *Environment International*, 158, pp. 106908. https://doi.org/10.1016/j.envint.2021.106908

Kaufmann, B. *et al.* (2021) 'In-situ determination of antimony isotope ratios in Sb minerals by femtosecond LA-MC-ICP-MS', *Journal of Analytical Atomic Spectrometry*, 36, pp. 1554-1567. https://doi.org/10.1039/D1JA00089F.

Bigham, J.M. *et al.* (1996) 'Schwertmannite and the chemical modeling of iron in acid sulfate waters', *Geochimica et Cosmochimica Acta*, 60(12), pp. 2111–2121. https://doi.org/10.1016/0016-7037(96)00091-9.

Biver, M., and Shotyk, W. (2012) 'Experimental study of the kinetics of ligand-promoted dissolution of stibnite (Sb2S3)', *Chemical Geology*, *294*, pp. 165-172. https://doi.org/10.1016/j.chemgeo.2011.11.009.

Biver, M. (2021) 'A Comprehensive Potentiometric Study of the Tartrate Complexes of Trivalent Arsenic, Antimony, and Bismuth in Aqueous Solution', *Inorganic Chemistry*, 60(23), pp. 18360–18369. https://doi.org/10.1021/acs.inorgchem.1c02962.

Bryan, A.L. *et al.* (2015) 'Zinc isotope fractionation during adsorption onto Mn oxyhydroxide at low and high ionic strength', *Geochimica et Cosmochimica Acta*, 157, pp. 182–197. https://doi.org/10.1016/j.gca.2015.01.026.

European Commission (2020) *'Communication From The Commission To The European Parliament, The Council, The European Economic And Social Committee And The Committee Of The Regions. Critical Raw Materials Resilience: Charting a Path towards greater Security and Sustainability*', Communication COM(2020)474.

Degryse, P. *et al.* (2015) 'Isotopic investigation into the raw materials of Late Bronze Age glass making', *Journal of Archaeological Science*, 62, pp. 153–160. https://doi.org/10.1016/j.jas.2015.08.004.

Degryse, P. *et al.* (2020) 'Isotopic evidence for the use of Caucasian antimony in Late Bronze Age glass making', *Journal of Archaeological Science*, 120, p. 105195. https://doi.org/10.1016/j.jas.2020.105195.

Essington, M.E. and Stewart, M.A. (2018) 'Adsorption of Antimonate, Sulfate, and Phosphate by Goethite: Reversibility and Competitive Effects', *Soil Science Society of America Journal*, 82(4), pp. 803–814. https://doi.org/10.2136/sssaj2018.01.0003.

Ferrari, C. *et al.* (2021) 'Correction for: A single-step purification method for the precise determination of antimony isotopic composition of environmental, geological and biological samples by HG-MC-ICP-MS', *Journal of Analytical Atomic Spectrometry*, 36(4), pp. 776–785. https://doi.org/10.1039/D1JA90048J

Ferrari, C. *et al.* (2022) 'Equilibrium mass-dependent isotope fractionation of antimony between stibnite and Sb secondary minerals: A first-principles study', *Chemical Geology*, 611, p. 121115. https://doi.org/10.1016/j.chemgeo.2022.121115.

Ferrari, C., et al. (2023) 'Antimony isotopic fractionation during Sb (III) oxidation to Sb (V): Biotic and abiotic processes.' *Chemical Geology* 641 (2023): 121788. https://doi.org/10.1016/j.chemgeo.2023.121788.

Filella, M., Belzile, N. and Chen, Y.-W. (2002) 'Antimony in the environment: a review focused on natural waters: I. Occurrence', *Earth-Science Reviews*, 57, pp. 125-176. https://doi.org/10.1016/S0012-8252(01)00070-8.

Filella, M., Williams, P.A. and Belzile, N. (2009) 'Antimony in the environment : knows and unknowns', *Environmental Chemistry*, 6, pp. 95–105. https://doi.org/10.1071/EN09007.

Goldberg, T. *et al.* (2009) 'Mo isotope fractionation during adsorption to Fe (oxyhydr)oxydes', *Geochimica et Cosmochimica Acta*, 73, pp. 6502–6516. https://doi.org/10.1016/j.gca.2009.08.004.

Gueguen, B. *et al.* (2018) 'Variable Ni isotope fractionation between Fe-oxyhydroxides and implications for the use of Ni isotopes as geochemical tracers', *Chemical Geology*, 481, pp. 38–52. https://doi.org/10.1016/j.chemgeo.2018.01.023.

Guo, W. *et al.* (2018) 'Environmental geochemical and spatial/temporal behavior of total and speciation of antimony in typical contaminated aquatic environment from Xikuangshan, China', *Microchemical Journal*, 137, pp. 181–189. https://doi.org/10.1016/j.microc.2017.10.010.

635 Guo, X. *et al.* (2014) 'Adsorption of antimony onto iron oxyhydroxides: Adsorption behavior
636 and surface structure', *Journal of Hazardous Materials*, 276, pp. 339–345.
637 http://dx.doi.org/10.1016/j.jhazmat.2014.05.025.

638 Hao, C. *et al.* (2021) 'Contrasting water–rock interaction behaviors of antimony and arsenic in
639 contaminated rivers around an antimony mine, Hunan Province, China', *Geochemistry*, 81(2),
640 p. 125748. https://doi.org/10.1016/j.chemer.2021.125748.

641 He, M. *et al.* (2019) 'Antimony speciation in the environment: Recent advances in
642 understanding the biogeochemical processes and ecological effects', *Journal of*
643 *Environmental Sciences*, 75, pp. 14–39. https://doi.org/10.1016/j.jes.2018.05.023.

644 Johnson, T. M., *et al.* (2022) 'A review of the development of Cr, Se, U, Sb, and Te isotopes
645 as indicators of redox reactions, contaminant fate, and contaminant transport in aqueous
646 systems', *Isotopic Constraints on Earth System Processes*, pp. 237-269.

647 Johnston, S. G., *et al.* (2020) 'Antimony and arsenic speciation, redox-cycling and contrasting
648 mobility in a mining-impacted river system', *Science of the Total Environment, 710*, p.
649 136354. https://doi.org/10.1016/j.scitotenv.2019.136354

650 Juillot, F. *et al.* (2008) 'Zn isotopic fractionation caused by sorption on goethite and 2-Lines
651 ferrihydrite', *Geochimica et Cosmochimica Acta*, 72(19), pp. 4886–4900.
652 https://doi.org/10.1016/j.gca.2008.07.007.

653 Komárek, M. *et al.* (2021) 'Metal isotope complexation with environmentally relevant
654 surfaces: Opening the isotope fractionation black box', *Critical Reviews in Environmental*
655 *Science & Technology*, pp. 1–31. https://doi.org/10.1080/10643389.2021.1955601.

656 Leuz, A.-K., Mönch, H. and Johnson, A. (2006) 'Sorption of Sb(III) and Sb(V) to Goethite:
657 Influence on Sb(III) Oxidation and Mobilization', *Environmental Science & Technology*,
658 40(23), pp. 7277–7282. https://doi.org/10.1021/es061284b.

659 Li, S. *et al.* (2021) 'A new purification method based on a thiol silica column for high
660 precision antimony isotope measurements', *Journal of Analytical Atomic Spectrometry*, 36,
661 pp. 157–164. https://doi.org/10.1039/D0JA00367K.

662 Li, Y. *et al.* (2016) 'Removal of antimonate and antimonite from water by schwertmannite
663 granules', *Desalination and Water Treatment*, pp. 1–14.
664 https://doi.org/10.1080/19443994.2016.1155176.

665 Liu, F. *et al.* (2015) 'Schwertmannite Synthesis through Ferrous Ion Chemical Oxidation
666 under Different H2O2 Supply Rates and Its Removal Efficiency for Arsenic from
667 Contaminated Groundwater', *PLOS ONE*, 10(9), p. e0138891.
668 https://doi.org/10.1371/journal.pone.0138891.

669 Liu, J. *et al.* (2020) 'Chromatographic purification of antimony for accurate isotope analysis
670 by MC-ICP-MS', *Journal of Analytical Atomic Spectrometry*, 35, pp. 1360–1367.
671 https://doi.org/10.1039/D0JA00136H.

672 Lobo, L. *et al.* (2012) 'Investigation of natural isotopic variation of Sb in stibnite ores via
673 multi-collector ICP-mass spectrometry - perspectives for Sb isotopic analysis of Roman
674 glass', *Journal of Analytical Atomic Spectrometry*, 27, pp. 1304–1310.
675 https://doi.org/10.1039/c2ja30062a.

676 Lobo, L. *et al.* (2013) 'Isotopic analysis of antimony using multi-collector ICP-mass
677 spectrometry for provenance determination of Roman glass', *Journal of Analytical Atomic*
678 *Spectrometry*, 28, pp. 1213–1219. https://doi.org/10.1039/c3ja50018g.

679 Lobo, L. *et al.* (2014) 'Copper and antimony isotopic analysis via multi-collector ICP-mass
680 spectrometry for provenancing ancient glass', *Journal of Analytical Atomic Spectrometry*,
681 29(1), pp. 58–64. https://doi.org/10.1039/C3JA50303H.

682 Manaka, M. *et al.* (2007) 'Natural attenuation of antimony in mine drainage water',
683 *Geochemical Journal*, 41(1), pp. 17–27. https://doi.org/10.2343/geochemj.41.17.

684 McComb, K.A., Craw, D. and McQuillan, A.J. (2007) 'ATR-IR Spectroscopic Study of
685 Antimonate Adsorption to Iron Oxide', *Langmuir*, 23(24), pp. 12125–12130.
686 https://doi.org/10.1021/la7012667.

687 Mitsunobu, S. *et al.* (2010) 'Antimony(V) Incorporation into Synthetic Ferrihydrite, Goethite,
688 and Natural Iron Oxyhydroxides', *Environmental Science & Technology*, 44(10), pp. 3712–
689 3718. https://doi.org/10.1021/es903901e.

690 Mitsunobu, S., Harada, T. and Takahashi, Y. (2006) 'Comparison of Antimony Behavior with
691 that of Arsenic under Various Soil Redox Conditions', *Environmental Science & Technology*,
692 40(23), pp. 7270–7276. https://doi.org/10.1021/es060694x.

693 Nagano, T. *et al.* (2011) 'Evaluation of the Affinity of Some Toxic Elements to
694 Schwertmannite in Natural Streams Contaminated with Acid Mine Drainage', *Water, Air, &*
695 *Soil Pollution*, 216(1), pp. 153–166. https://doi.org/10.1007/s11270-010-0523-9.

696 Parks, G.A. (1965) 'The isoelectric points of solid oxides, solid hydroxides, and aqueous
697 hydroxo complex systems', *Chemical Reviews*, 65(2), pp. 177–198.
698 https://doi.org/10.1021/cr60234a002

699 Pokrovsky, O.S. *et al.* (2014) 'Germanium isotope fractionation during Ge adsorption on
700 goethite and its coprecipitation with Fe oxy(hydr)oxides', *Geochimica et Cosmochimica Acta*,
701 131, pp. 138–149. https://doi.org/10.1016/j.gca.2014.01.023.

702 Qi, P. and Pichler, T. (2016) 'Sequential and simultaneous adsorption of Sb(III) and Sb(V) on
703 ferrihydrite: Implications for oxidation and competition', *Chemosphere*, 145, pp. 55–60.
704 https://doi.org/10.1016/j.chemosphere.2015.11.057.

705 Qi, P. and Pichler, T. (2017) 'Competitive adsorption of As(III), As(V), Sb(III) and Sb(V)
706 onto ferrihydrite in multi-component systems: Implications for mobility and distribution',
707 *Journal of Hazardous Materials*, 330, pp. 142–148.
708 https://doi.org/10.1016/j.jhazmat.2017.02.016.

Regenspurg, S., Brand, A. and Peiffer, S. (2004) 'Formation and stability of schwertmannite in acidic mining lakes', *Geochimica et Cosmochimica Acta*, 68(6), pp. 1185–1197. https://doi.org/10.1016/j.gca.2003.07.015.

Rastegari, M., et al. (2022). Antimony (V) incorporation into schwertmannite: critical insights on antimony retention in acidic environments. *Environmental science & technology*, *56*(24), 17776-17784

Resongles, E. *et al.* (2013) 'Fate of Sb(V) and Sb(III) species along a gradient of pH and oxygen concentration in the Carnoulès mine waters (Southern France)', *Environmental Science Processes and Impacts*, 15, pp. 1536–1544. https://doi.org/10.1039/c3em00215b.

Resongles, E. *et al.* (2015) 'Antimony isotopic composition in river waters affected by ancient mining activity', *Talanta*, 144, pp. 851–861. http://dx.doi.org/10.1016/j.talanta.2015.07.013.

Resongles, E. *et al.* (2021) 'Antimony isotopic composition in stream waters impacted by acid mine drainage', Goldschmidt2021, Virtual, 4-9 July 2021. https://doi.org/10.7185/gold2021.5268

Rouxel, O., Ludden, J. and Fouquet, Y. (2003) 'Antimony isotope variations in natural systems and implications for their use as geochemical tracers', *Chemical Geology*, 200, pp. 25–40. https://doi.org/10.1016/S0009-2541(03)00121-9.

Scheinost, A.C. *et al.* (2006) 'Quantitative antimony speciation in shooting-range soils by EXAFS spectroscopy', *Geochimica et Cosmochimica Acta*, 70(13), pp. 3299–3312. https://doi.org/10.1016/j.gca.2006.03.020.

Schoepfer, V. A., & Burton, E. D. (2021) 'Schwertmannite: a review of its occurrence, formation, structure, stability and interactions with oxyanions', *Earth-Science Reviews*, 221, p. 103811. https://doi.org/10.1016/j.earscirev.2021.103811.

Schwertmann, U. and Cornell, R.M. (2000) *Iron Oxides in the Laboratory - Preparation and characterization*. Second Edition. WILEY-VCH.

Shan, J., *et al.* (2023). Antimony immobilization mechanism on schwertmannite: Insights from the microstructure of schwertmannite. *Geochimica et Cosmochimica Acta*, *359*, 71-83.

Sun, G. *et al.* (2021) 'Precise analysis of antimony isotopic composition in geochemical materials by MC-ICP-MS', *Chemical Geology*, 582, p. 120459. https://doi.org/10.1016/j.chemgeo.2021.120459.

Tanimizu, M. *et al.* (2011) 'Determination of natural isotopic variation in antimony using inductively coupled plasma mass spectrometry for an uncertainty estimation of the standard atomic weight of antimony', *Geochemical Journal*, 45, pp. 27–32.

Tella, M., & Pokrovski, G. S. (2012) 'Stability and structure of pentavalent antimony complexes with aqueous organic ligands', *Chemical Geology*, *292*, pp. 57-68.

Teng, F.-Z., Dauphas, N. and Watkins, J.M. (2017) 'Non-Traditional Stable Isotopes: Retrospective and Prospective', *Reviews in Mineralogy and Geochemistry*, 82(1), pp. 1–26. https://doi.org/10.2138/rmg.2017.82.1.

U.S. Geological Survey (2018) ‘Antimony - Historical Statistics (Data series 140 - 2018 update)’. Available at: https://www.usgs.gov/media/files/antimony-historical-statistics-data-series-140. Last access on 27/7/2023.

U.S. Geological Survey (2022) *2022 Final List of Critical Minerals*. Notices Federal Register / Vol. 87, No. 37.

Veldhuizen, H.J., MacKinney, J.S., Johnson, T.M. ‘Kinetic Fractionation of Antimony Isotopes during Reduction by Sulfide.’ *ACS Earth Space Chem*. **7** (2023): 2603−2612. https://doi.org/10.1021/acsearthspacechem.3c00269

Wang, S.-J. and Wasylenki, L.E. (2017) ‘Experimental constraints on reconstruction of Archean seawater Ni isotopic composition from banded iron formations’, *Geochimica et Cosmochimica Acta*, 206, pp. 137–150. https://doi.org/10.1016/j.gca.2017.02.023.

Wang, X. *et al.* (2011) ‘Antimony distribution and mobility in rivers around the world’s largest antimony mine of Xikuangshan, Hunan Province, China’, *Microchemical Journal*, 97(1), pp. 4–11. https://doi.org/10.1016/j.microc.2010.05.011.

Wasylenki, L.E. *et al.* (2011) ‘The molecular mechanism of Mo isotope fractionation during adsorption to birnessite’, *Geochimica et Cosmochimica Acta*, 75(17), pp. 5019–5031. https://doi.org/10.1016/j.gca.2011.06.020.

Wasylenki, L.E. *et al.* (2015) ‘Ni isotope fractionation during sorption to ferrihydrite: Implications for Ni in banded iron formations’, *Chemical Geology*, 400, pp. 56–64. https://doi.org/10.1016/j.chemgeo.2015.02.007.

WHO, World Health Organization (2011) ‘Fourth Edition. Guidelines for drinking-water quality

WHO Chronicle’, 38 (4), pp. 104-108.

Wiederhold, J.G. (2015) ‘Metal Stable Isotope Signatures as Tracers in Environmental Geochemistry’, *Environmental Science & Technology*, 49(5), pp. 2606–2624. https://doi.org/10.1021/es504683e.

Wu, D., Pichler, T. (2016) ‘Preservation of co-occurring As, Sb and Se species in water samples with EDTA and acidification’, *Geochemistry: Exploration, Environment, Analysis*, 16, p.p. 117–125. https://doi.org/10.1144/geochem2015-369.

Xu, W. *et al.* (2020) ‘Selenium isotope fractionation during adsorption by Fe, Mn and Al oxides’, *Geochimica et Cosmochimica Acta*, 272, pp. 121–136. https://doi.org/10.1016/j.gca.2020.01.001.

Yan, X. *et al.* (2021) ‘Cadmium Isotope Fractionation during Adsorption and Substitution with Iron (Oxyhydr)oxides’, *Environmental Science & Technology*, 55(17), pp. 11601–11611. https://doi.org/10.1021/acs.est.0c06927.

Zhou, W. *et al.* (2022) ‘Antimony isotope fractionation during adsorption on aluminum oxides’, *Journal of Hazardous Materials*, 429, p. 128317. https://doi.org/10.1016/j.jhazmat.2022.128317.

785 Zhou, W. *et al.* (2023) ‘Antimony Isotope Fractionation Revealed from EXAFS during
786 Adsorption on Fe (Oxyhydr)oxides’, *Environmental Science & Technology*, 57, pp.
787 9353−9361. https://doi.org/10.1021/acs.est.3c01906